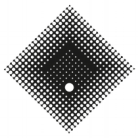

Numerical study of circular double-skin concrete-filled aluminum tubular stub columns

Patel, V. I., Liang, Q. Q. and Hadi, M. N. S. (2019). Numerical study of circular double-skin concrete-filled aluminum tubular stub columns. *Engineering Structures*, 197: 109418.

Figures and tables

Table 1 Material properties of aluminum.

Specimens	$\sigma_{0.2}$ (MPa)	σ_{au} (MPa)	E_0 (GPa)	n	Ref.
C4	267.9	282.9	64.9	5.0	[7]
CHS2	238.4	259.1	66.1	5.0	

Table 2 Ultimate axial loads of circular DCFAT stub columns under axial compression.

Specimens	$D_o \times t_o$ (mm)	$D_i \times t_i$ (mm)	$f_c^{'}$ (MPa)	$\sigma_{0.2o}$ (MPa)	σ_{auo} (MPa)	E_{0o} (GPa)	$\sigma_{0.2i}$ (MPa)	σ_{aui} (MPa)	E_{0i} (GPa)	$P_{u\exp}$ (kN)	$P_{u\text{num}}$ (kN)	$\frac{P_{u\text{num}}}{P_{u\exp}}$	Ref.
C3C1-C40	120.0×2.48	50.0×3.09	44.8	253.1	264.7	66.5	238.4	259.1	66.1	712.4	717.0	1.007	[7]
C3C1-C70	119.7×2.41	49.9×3.09	70.2	253.1	264.7	66.5	238.4	259.1	66.1	822.9	911.7	1.108	
C3C1-C100	119.3×2.45	49.9×3.10	106.0	253.1	264.7	66.5	238.4	259.1	66.1	1101.1	1199.2	1.089	
C3C2-C40	119.7×2.49	76.1×2.13	44.8	253.1	264.7	66.5	237.0	256	64.9	595.7	578.8	0.972	
C3C2-C70	119.6×2.50	76.1×2.05	70.2	253.1	264.7	66.5	237.0	256	64.9	701.0	708.6	1.011	
C3C2-C100	120.4×2.32	76.0×2.04	106.0	253.1	264.7	66.5	237.0	256	64.9	904.4	911.7	1.008	
C4C1-C40	149.9×2.50	50.0×3.17	44.8	267.9	282.9	64.9	238.4	259.1	66.1	1064.5	1043.4	0.980	
C4C1-C70	150.1×2.49	50.1×3.19	70.2	267.9	282.9	64.9	238.4	259.1	66.1	1438.7	1397.8	0.972	
C4C1-C100	150.0×2.50	50.0×3.13	106.0	267.9	282.9	64.9	238.4	259.1	66.1	1980.9	1898.1	0.958	
C4C2-C40	150.2×2.53	76.1×1.95	44.8	267.9	282.9	64.9	237.0	256	64.9	936.5	697.4	0.974	
C4C2-C70	150.0×2.51	75.9×2.08	70.2	267.9	282.9	64.9	237.0	256	64.9	1210.7	975.7	1.001	
C4C2-C100	149.8×2.54	76.1×2.02	106.0	267.9	282.9	64.9	237.0	256	64.9	1566.1	1437.5	1.026	
C5C1-C40	150.0×5.14	49.9×3.00	44.8	267.9	251.9	65.8	238.4	259.1	66.1	1465.8	1416.8	0.967	
C5C1-C70	150.3×4.98	50.0×3.07	70.2	267.9	251.9	65.8	238.4	259.1	66.1	1675.4	1708.5	1.020	
C5C1-C100	150.1×4.99	49.9×3.18	106.0	267.9	251.9	65.8	238.4	259.1	66.1	2095.0	2230.0	1.064	
C5C2-C40	150.2×4.94	76.0×2.09	44.8	267.9	251.9	65.8	237.0	256	64.9	1256.3	1213.0	0.975	
C5C2-C70	150.2×4.93	76.1×2.09	70.2	267.9	251.9	65.8	237.0	256	64.9	1368.0	1488.7	1.097	
C5C2-C100	150.3×4.94	76.1×2.12	106.0	267.9	251.9	65.8	237.0	256	64.9	1856.8	1886.7	1.023	
C6C1-C40	160.4×4.01	50.0×3.14	44.8	254.2	272.9	66.6	238.4	259.1	66.1	1373.3	1473.1	1.079	
C6C1-C70	160.5×4.02	50.0×3.15	70.2	254.2	272.9	66.6	238.4	259.1	66.1	1786.0	1890.3	1.064	
C6C1-C100	160.5×4.04	50.0×3.17	106.0	254.2	272.9	66.6	238.4	259.1	66.1	2540.0	2477.0	0.979	
C6C2-C40	160.5×4.02	76.1×2.02	44.8	254.2	272.9	66.6	237.0	256	64.9	1342.7	1295.0	0.971	
C6C2-C70	160.4×4.02	76.0×2.04	70.2	254.2	272.9	66.6	237.0	256	64.9	1472.3	1644.6	1.123	
C6C2-C100	160.7×4.02	76.1×2.00	106.0	254.2	272.9	66.6	237.0	256	64.9	2099.8	2137.1	1.022	
Mean												1.020	
Standard deviation (SD)												0.050	
Coefficient of variation (COV)												0.050	

Table 3 Lateral confining pressures on the sandwiched concrete confined by circular carbon steel tubes and aluminum tubes.

Specimens	$P_{ue\exp}$ (kN)	Hu and Su model [36]			Proposed model Eq. (22)		
		f_{rp1} (MPa)	P_{ufrp1} (kN)	$\frac{P_{ufrp1}}{P_{u\exp}}$	f_{rp} (MPa)	P_{ufrp} (kN)	$\frac{P_{ufrp}}{P_{u\exp}}$
C3C1-C40	712.4	3.760	853.9	1.199	1.11	717.0	1.007
C3C1-C70	822.9	3.758	1055.0	1.282	1.05	911.7	1.108
C3C1-C100	1101.1	3.764	1338.3	1.215	1.09	1199.2	1.089
C3C2-C40	595.7	0.318	601.0	1.009	0.61	578.8	0.972
C3C2-C70	701.0	0	722.8	1.031	0.54	708.6	1.011
C3C2-C100	904.4	0.065	925.0	1.023	0.51	911.7	1.008
C4C1-C40	1064.5	3.882	1309.9	1.231	0.92	1043.4	0.980
C4C1-C70	1438.7	3.892	1674.0	1.164	0.93	1397.8	0.972
C4C1-C100	1980.9	3.876	2167.6	1.094	0.93	1898.1	0.958
C4C2-C40	936.5	0.049	915.8	0.978	0.60	697.4	0.974
C4C2-C70	1210.7	0.783	1250.9	1.033	0.71	975.7	1.001
C4C2-C100	1566.1	0.404	1621.0	1.035	0.64	1437.5	1.026
C5C1-C40	1465.8	4.268	1528.7	1.043	2.87	1416.8	0.967
C5C1-C70	1675.4	4.258	1848.5	1.103	2.74	1708.5	1.020
C5C1-C100	2095.0	4.329	2334.8	1.114	2.77	2230.0	1.064
C5C2-C40	1256.3	0	1173.7	0.934	1.67	1213.0	0.975
C5C2-C70	1368.0	0	1449.8	1.060	1.66	1488.7	1.097
C5C2-C100	1856.8	0	1845.8	0.994	1.70	1886.7	1.023
C6C1-C40	1373.3	3.914	1641.0	1.195	1.66	1473.1	1.079
C6C1-C70	1786.0	3.921	2058.4	1.153	1.67	1890.3	1.064
C6C1-C100	2540.0	3.935	2653.9	1.045	1.69	2477.0	0.979
C6C2-C40	1342.7	0	1276.6	0.951	0.81	1295.0	0.971
C6C2-C70	1472.3	0	1624.6	1.103	0.83	1644.6	1.123
C6C2-C100	2099.8	0	2120.1	1.010	0.78	2137.1	1.022
Mean				1.083			1.020
Standard deviation (SD)				0.094			0.050
Coefficient of variation (COV)				0.087			0.050

Table 4 Dimensions and material variables of circular DCFAT stub columns used in the parametric studies

Column	D_o (mm)	t_o (mm)	D_o/t_o	D_i (mm)	t_i (mm)	D_i/t_i	$\sigma_{0.2o}$, $\sigma_{0.2i}$ (MPa)	σ_{auo}, σ_{aui} (MPa)	f_c' (MPa)
C1	500	10	50	240	10	24.0	250	270	50
C2	600	10	60	180	7	25.7	250	260	40
C3	600	10	60	240	7	34.3	250	260	40
C4	600	10	60	300	7	42.9	250	260	40
C5	600	10	60	360	7	51.4	250	260	40
C6	450	10	45	200	6.67	30.0	270	280	65
C7	550	10	55	200	6.67	30.0	270	280	65
C8	600	10	60	200	6.67	30.0	270	280	65
C9	500	10	50	200	13.33	15.0	240	260	80
C10	500	10	50	200	8	25.0	240	260	80
C11	500	10	50	200	5.71	35.0	240	260	80
C12	700	14	50	350	10	35.0	220	250	100
C13	700	14	50	350	10	35.0	240	260	100
C14	700	14	50	350	10	35.0	250	260	100
C15	700	14	50	350	10	35.0	260	280	100
C16	550	10	55	250	10	25.0	250	260	40
C17	550	10	55	250	10	25.0	250	260	65
C18	550	10	55	250	10	25.0	250	260	80
C19	550	10	55	250	10	25.0	250	260	100
C20	300	6	50	150	5	30.0	270	280	65

Table 5 Comparison of experimental ultimate axial loads of DCFAT short columns with those calculated by the codified methods and design model.

Specimens	L (mm)	P_u (kN)	AISC 316-16 [54]		Eurocode 4 [55]		Liang [38]	
			$P_{u\mathrm{AISC}}$ (kN)	$\frac{P_{u\mathrm{AISC}}}{P_u}$	$P_{u\mathrm{EC4}}$ (kN)	$\frac{P_{u\mathrm{EC4}}}{P_u}$	$P_{u\mathrm{Liang}}$ (kN)	$\frac{P_{u\mathrm{Liang}}}{P_u}$
C3C1-C40	360	712.4	699.1	0.981	757.4	1.063	690.0	0.969
C3C1-C70	360	822.9	893.9	1.086	955.0	1.160	893.1	1.085
C3C1-C100	360	1101.1	1174.4	1.067	1243.2	1.129	1189.8	1.081
C3C2-C40	360	595.7	595.7	1.000	619.4	1.040	553.1	0.929
C3C2-C70	360	701.0	730.4	1.042	759.3	1.083	695.0	0.991
C3C2-C100	360	904.4	933.2	1.032	970.3	1.073	906.6	1.002
C4C1-C40	450	1064.5	1039.6	0.977	1142.2	1.073	1031.6	0.969
C4C1-C70	450	1438.7	1393.0	0.968	1502.5	1.044	1403.5	0.976
C4C1-C100	450	1980.9	1885.4	0.952	2008.8	1.014	1922.4	0.970
C4C2-C40	450	936.5	932.7	0.996	1010.6	1.079	893.3	0.954
C4C2-C70	450	1210.7	1225.1	1.012	1308.4	1.081	1204.0	0.994
C4C2-C100	450	1566.1	1624.6	1.037	1720.6	1.099	1622.1	1.036
C5C1-C40	450	1465.8	1182.1	0.806	1329.5	0.907	1337.5	0.912
C5C1-C70	450	1675.4	1501.7	0.896	1648.2	0.984	1663.3	0.993
C5C1-C100	450	2095.0	1960.6	0.936	2112.6	1.008	2147.0	1.025
C5C2-C40	450	1256.3	1069.1	0.851	1170.1	0.931	1126.2	0.896
C5C2-C70	449	1368.0	1331.5	0.973	1436.4	1.050	1401.6	1.025
C5C2-C100	450	1856.8	1707.5	0.920	1820.3	0.980	1799.0	0.969
C6C1-C40	480	1373.3	1303.6	0.949	1462.8	1.065	1370.9	0.998
C6C1-C70	480	1786.0	1699.4	0.952	1862.1	1.043	1788.1	1.001
C6C1-C100	480	2540.0	2255.6	0.888	2428.0	0.956	2375.0	0.935
C6C2-C40	480	1342.7	1197.2	0.892	1320.8	0.984	1191.8	0.888
C6C2-C70	480	1472.3	1527.7	1.038	1655.7	1.125	1541.0	1.047
C6C2-C100	480	2099.8	1998.5	0.952	2137.8	1.018	2034.1	0.969
C1	1500	11835.6	12101.4	1.004	12988.1	1.078	11614.8	0.964
C2	1800	13619.1	14657.9	1.035	16453.6	1.162	13914.7	0.982
C3	1800	13453.6	14235.7	1.038	15770.2	1.150	13385.7	0.976
C4	1800	13008.6	13598.5	1.095	14805.3	1.192	12156.8	0.979
C5	1800	12909.2	12746.5	1.090	13551.4	1.159	11400.7	0.975
C6	1350	11769.5	11853.4	1.012	12841.9	1.096	11668.8	0.996
C7	1650	16444.6	17357.5	1.047	18935.3	1.143	16534.6	0.998
C8	1800	18985.6	20473.3	1.056	22355.2	1.153	19374.5	0.999
C9	1500	16330.3	16935.7	1.010	18038.5	1.076	16439.2	0.981
C10	1500	15752.9	16217.7	1.014	17447.5	1.091	15854.3	0.992
C11	1500	15588.7	15896.0	1.037	17183.7	1.121	15431.7	1.007
C12	2100	32495.8	33541.6	1.049	35610.1	1.114	31958.4	0.999
C13	2100	33182.5	34358.7	1.055	36475.4	1.120	32615.9	1.001
C14	2100	33512.9	34767.2	1.058	36906.8	1.123	32944.7	1.003
C15	2100	33868.9	35175.7	1.061	37337.5	1.126	33273.4	1.004
C16	1650	12154.4	12644.3	1.017	13729.2	1.105	11915.8	0.959
C17	1650	16038.4	16718.1	1.025	17896.4	1.097	15987.0	0.980
C18	1650	18415.2	19162.5	1.025	20408.0	1.091	18429.8	0.985
C19	1650	21560.4	22421.5	1.027	23767.0	1.088	21686.8	0.993
C20	900	5026.1	5042.7	1.006	5385.8	1.074	4930.7	0.983
Mean				0.999		1.076		0.986
Standard deviation (SD)				0.063		0.064		0.039
Coefficient of variation (COV)				0.063		0.059		0.039

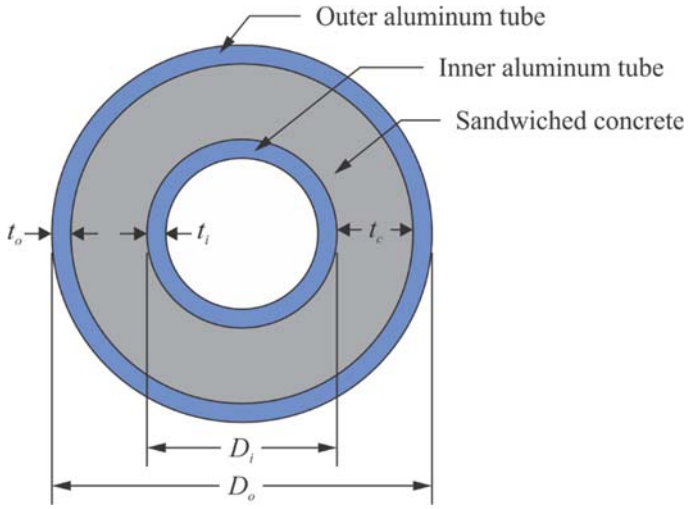

Fig. 1. Circular DCFAT column cross-section.

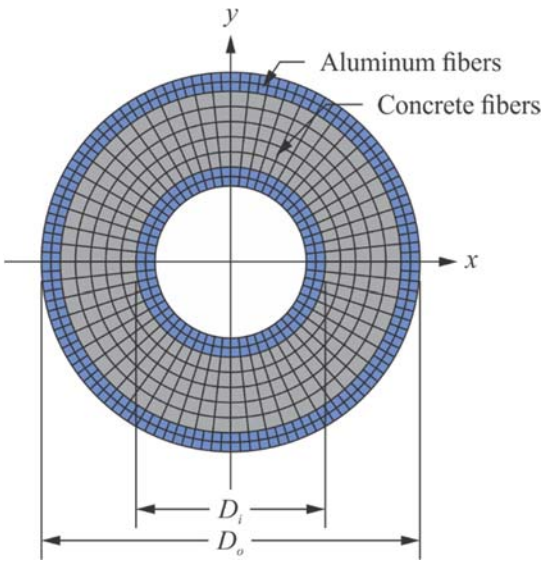

Fig. 2. Typical fiber mesh of circular DCFAT column.

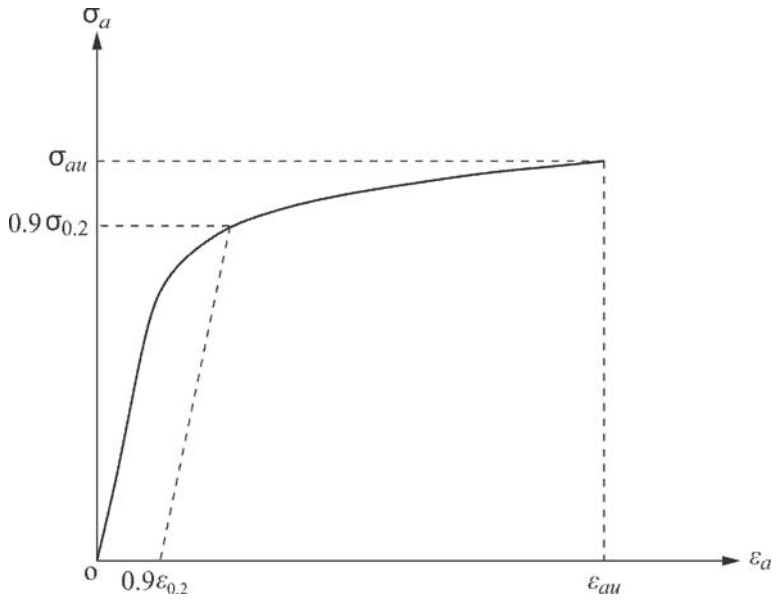

Fig. 3. Stress-strain curve for aluminum.

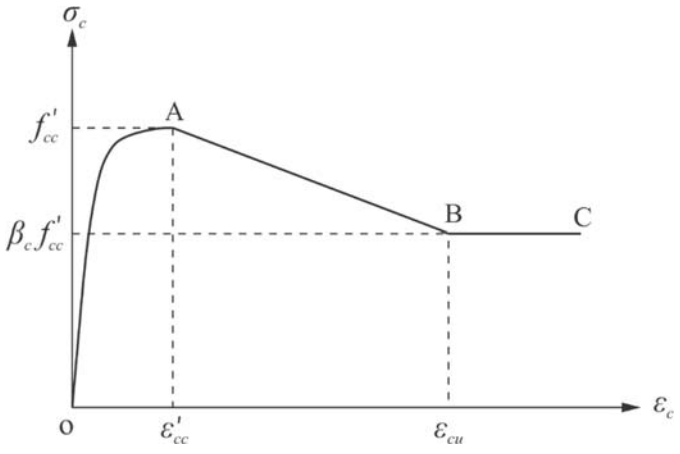

Fig. 4. Stress-strain curve for double-skin confined concrete.

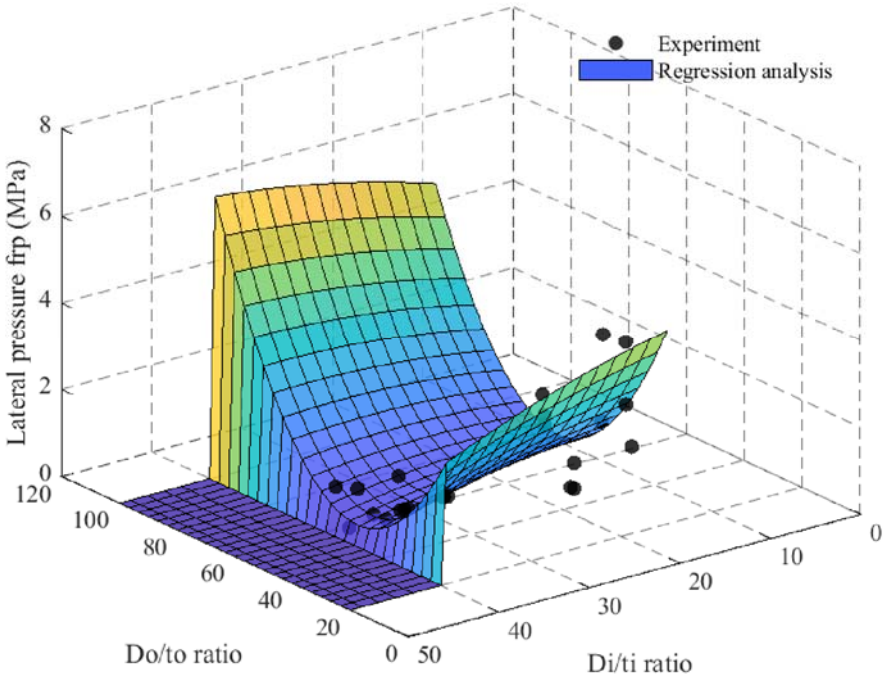

Fig. 5. Regression analysis for computing the lateral confining pressures from the experimental results [7].

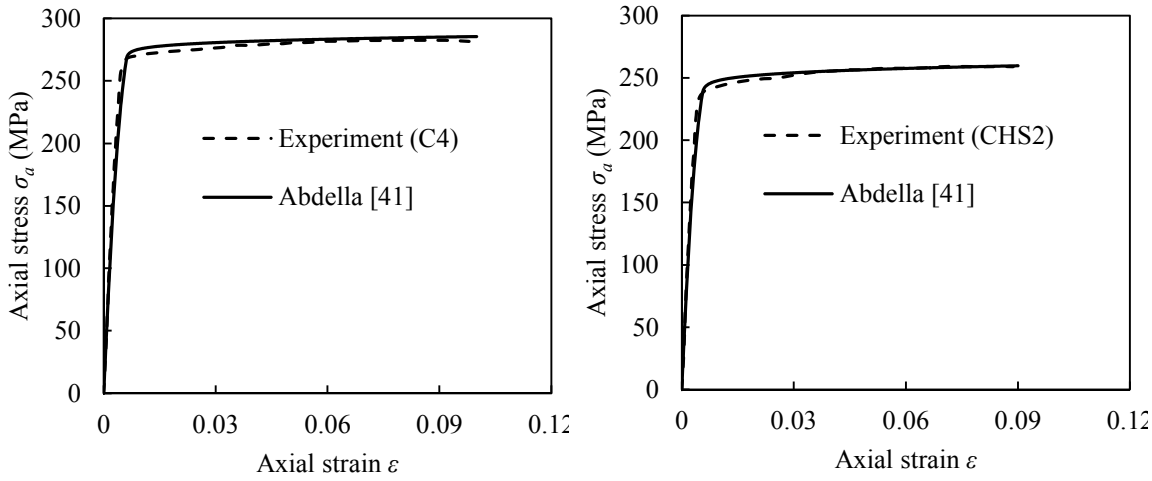

Fig. 6. Comparison of numerically captured and tested stress-strain responses of aluminum.

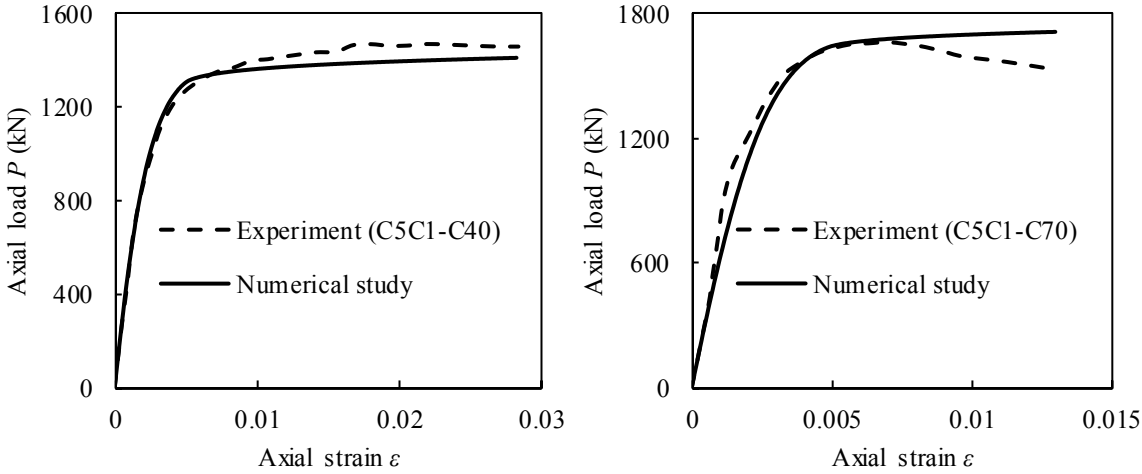

Fig. 7. Comparison of computed and experimental load-strain responses.

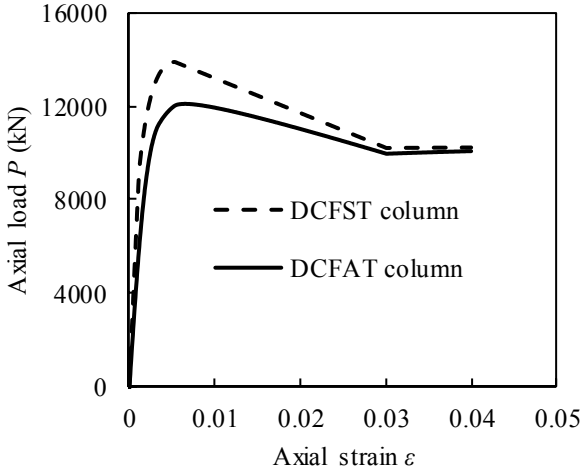

Fig. 8. Comparison of axial load-strain responses of circular DCFAT and DCFST columns.

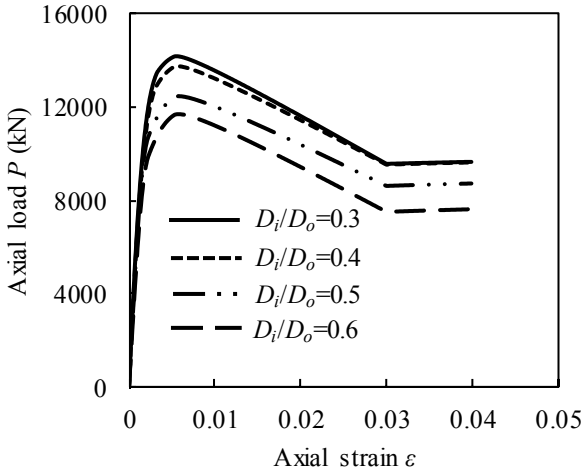

Fig. 9. Effect of D_i/D_o ratio on axial load-strain responses of circular DCFAT columns.

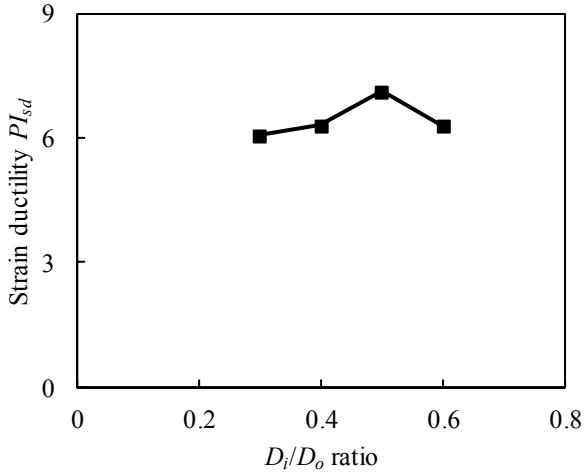

Fig. 10. Effect of D_i/D_o ratio on strain ductility PI_{sd}.

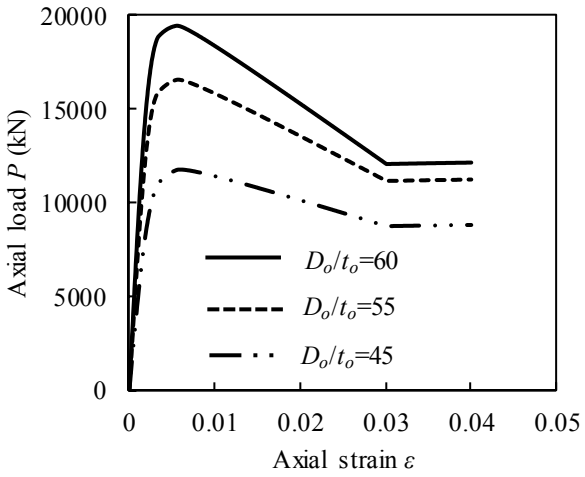

Fig. 11. Effect of D_o/t_o ratio on axial load-strain responses.

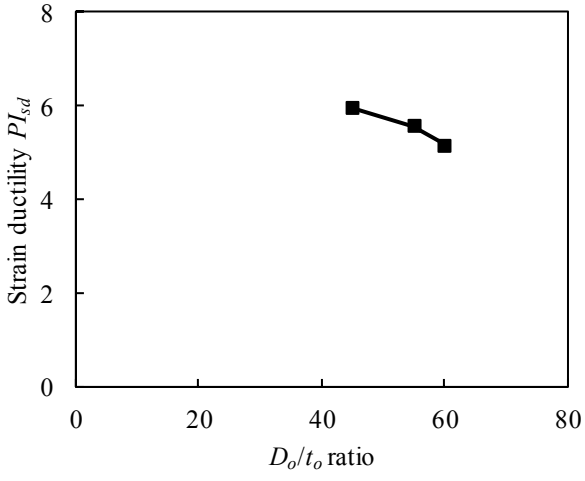

Fig. 12. Effect of D_o/t_o ratio on strain ductility PI_{sd}.

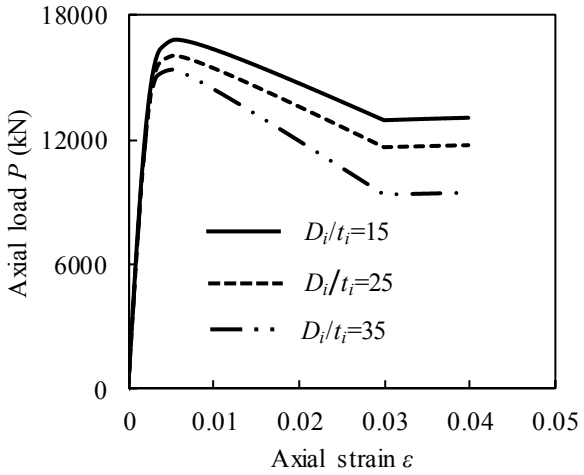

Fig. 13. Effect of D_i/t_i ratio on axial load-strain responses.

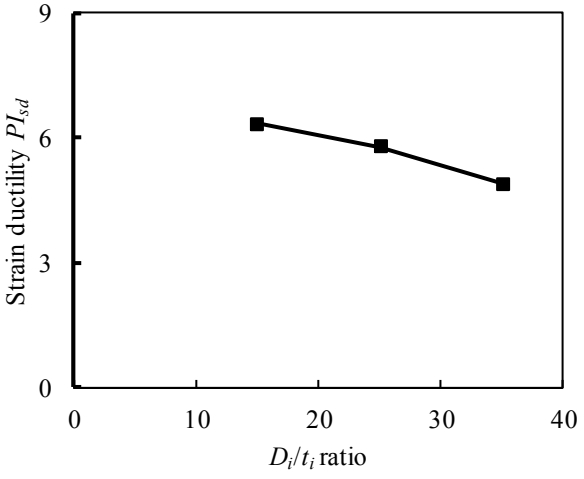

Fig. 14. Effect of D_i/t_i ratio on strain ductility PI_{sd}.

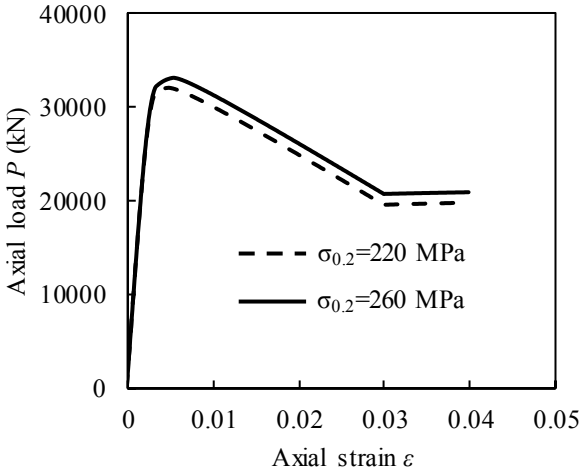

Fig. 15. Effect of aluminum strength on axial load-strain responses.

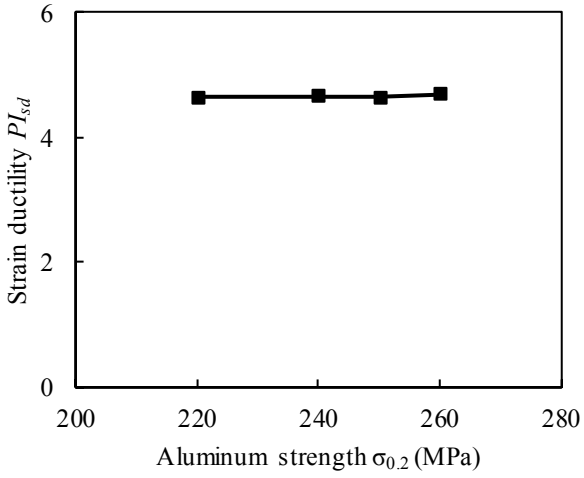

Fig. 16. Effect of aluminum strength on strain ductility PI_{sd} of circular DCFAT columns.

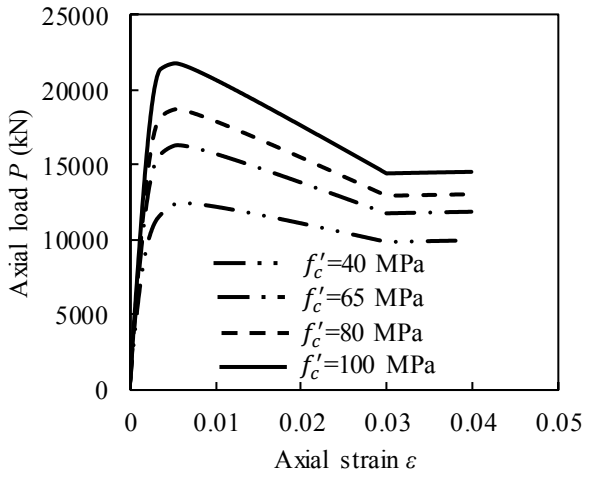

Fig. 17. Effect of concrete strength $f_c^{'}$ on load-strain responses.

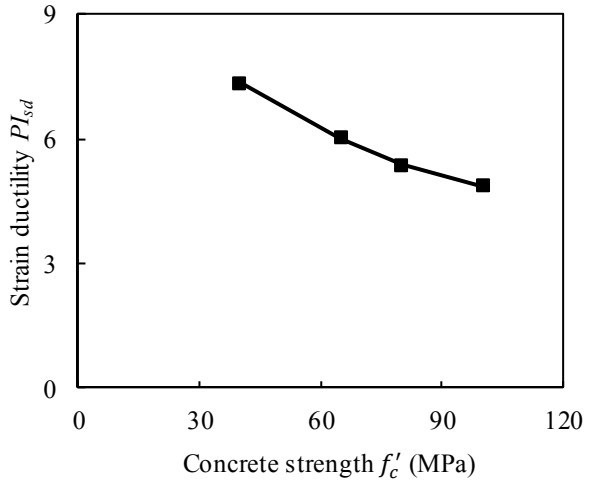

Fig. 18. Effect of concrete strength $f_c^{'}$ on strain ductility PI_{sd} of circular DCFAT columns.